

PL-TR-96-2178(IV)

RADAR STUDIES OF AVIATION HAZARDS: Part 4, Utility Of WSR-88D Doppler Spectrum Width

Alan R. Bohne

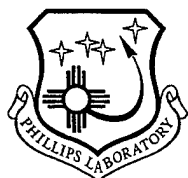
**Hughes STX Corporation
c/o OL-AA PL/GPAB
29 Randolph Road
Hanscom AFB, MA 01731-3010**

15 July, 1996

DTIC QUALITY INSPECTED 2

Scientific Report No. 3

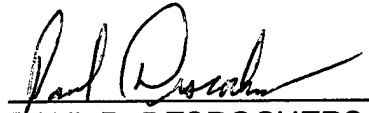
APPROVED FOR PUBLIC RELEASE; DISTRIBUTION UNLIMITED.

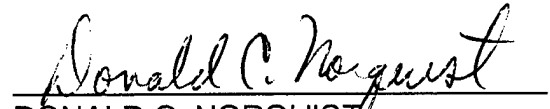


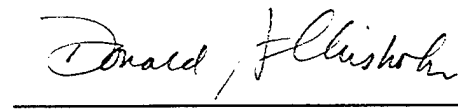
**PHILLIPS LABORATORY
Directorate of Geophysics
AIR FORCE MATERIEL COMMAND
HANSCOM AIR FORCE BASE, MA 01731-3010**

19970206 122

"This technical report has been reviewed and is approved for publication."


PAUL R. DESROCHERS
Contract Manager


DONALD C. NORQUIST
Acting Chief, Satellite Analysis and Weather
Prediction Branch
Atmospheric Sciences Division


DONALD A. CHISHOLM, Acting Director
Atmospheric Sciences Division

This report has been reviewed by the ESC Public Affairs Office (PA) and is releasable to the National Technical Information Service (NTIS).

Qualified requestors may obtain additional copies from the Defense Technical Information Center (DTIC). All others should apply to the National Technical Information Service (NTIS).

If your address has changed, or if you wish to be removed from the mailing list, or if the addressee is no longer employed by your organization, please notify PL/IM, 29 Randolph Road, Hanscom AFB, MA 01731-3010. This will assist us in maintaining a current mailing list.

Do not return copies of this report unless contractual obligations or notices on a specific document requires that it be returned.

REPORT DOCUMENTATION PAGE			Form Approved OMB No. 0704-0188	
Public reporting burden for this collection of information is estimated to average 1 hour per response, including the time for reviewing instructions, searching existing data sources, gathering and maintaining the data needed, and completing and reviewing the collection of information. Send comments regarding this burden estimate or any other aspect of this collection of information, including suggestions for reducing this burden, to Washington Headquarters Services, Directorate for Information Operations and Reports, 1215 Jefferson Davis Highway, Suite 1204, Arlington, VA 22202-4302, and to the Office of Management and Budget, Paperwork Reduction Project (0704-0188), Washington, DC 20503.				
1. AGENCY USE ONLY (Leave blank)		2. REPORT DATE 15 July 1996		3. REPORT TYPE AND DATES COVERED Scientific No. 3
4. TITLE AND SUBTITLE RADAR STUDIES OF AVIATION HAZARDS: Part 4. Utility of WSR-88D Doppler Spectrum Width			5. FUNDING NUMBERS F19628-93-C-0054 PE63707F PR 2781 TA GT WU MA	
6. AUTHOR(S) Alan R. Bohne				
7. PERFORMING ORGANIZATION NAME(S) AND ADDRESS(ES) Hughes STX Corporation c/o OL-AA PL/GPAB 29 Randolph Road Hanscom AFB, MA 01731-3010			8. PERFORMING ORGANIZATION REPORT NUMBER Hughes STX Scientific Report #11	
9. SPONSORING/MONITORING AGENCY NAME(S) AND ADDRESS(ES) Phillips Laboratory 29 Randolph Road Hanscom AFB, MA 01731-3010 Contract Manager: Paul R. Desrochers/GPAB			10. PERFORMING ORGANIZATION REPORT NUMBER PL-TR-96-2178(IV)	
11. SUPPLEMENTARY NOTES				
12a. DISTRIBUTION/AVAILABILITY STATEMENT Approved for public release; distribution unlimited			12b. DISTRIBUTION CODE	
13. ABSTRACT (Maximum 200 words) The behavior of the WSR-88D Doppler spectrum width parameter in hazardous storms is investigated for a variety of geographical locations. Analyses employ 3D visualization to identify the major associations between regions of high spectrum width and storm precipitation structures. Also, Doppler spectrum width is correlated with other collocated radar measurables on a radar sample volume scale to observe data interdependencies. The spectrum width is found useful for the detection of very large hail, and for surface wind shift features such as gust fronts and thin lines. Often, the spectrum width signatures are more readily detected than those traditionally employed. It is also useful for identifying data artifacts such as clutter, sidelobe contamination, incorrect range placement, insufficient SNR thresholding, and potential receiver saturation events. Automated methods for removing most artifacts appear to be feasible, and incorporation of spectrum width into automated detection routines is urged.				
14. SUBJECT TERMS Doppler weather radar, Doppler spectrum width, wind shift lines, WSR-88D data artifacts, hail storm structure			15. NUMBER OF PAGES 38	
			16. PRICE CODE	
17. SECURITY CLASSIFICATION Unclassified	18. SECURITY CLASSIFICATION OF THIS PAGE Unclassified	19. SECURITY CLASSIFICATION OF ABSTRACT Unclassified	20. LIMITATION OF ABSTRACT Unclassified	

Table of Contents

1	INTRODUCTION	1
3	CORRELATION OF SPW AND COLLOCATED Z AND V	17
4	WSR-88D PROBLEM AREAS	29
5	SUMMARY	32
6	BIBLIOGRAPHY	33

1 INTRODUCTION

This effort is focused on determining whether there is useful information within the WSR-88D Doppler spectrum width data (SPW) that could be exploited to provide new methods for detecting or forecasting storm features and hazards. The SPW is not a parameter that easily contributes to the description of storm winds or precipitation structures, since it is a measure of the distribution of the Doppler radial velocities of the scatterers within the radar pulse volume. During casual observation it often appears disassociated from storm structures, and is thus infrequently utilized in storm interpretation. However, when properly interpreted, the SPW is a simple and efficient source of additional information that provides insight into storm structure and processes.

The SPW is a measure of the dispersion, or scatter, of precipitation radial velocities about the Doppler mean velocity (V). As such, the SPW estimate is sensitive to a number of radar and meteorological factors that may combine to increase its value. These primarily include the radar pulse volume width and length, the gradients of the precipitation mean velocity (V) and reflectivity factor (Z), and turbulence. The time on target (e.g. scan rate, PRF), amount and performance of clutter filtering, and low signal-to-noise (SNR) ratio also affect the retrieved SPW estimate. Indeed, in many analyses (e.g. turbulence), the determination of the contributing factors to the SPW may be as relevant as the SPW measurement itself. Thus, depending upon the intended use of the SPW data, generally the "value" as well as the "origin" must be considered for meaningful interpretation.

In terms of operational utility, SPW has many advantages. For example, it is a simply estimated scalar quantity that is automatically provided by the WSR-88D. Also, it is highly localized and enhanced by local wind shears, reflectivity gradients, and turbulence. Thus, by observing the "patterns" of SPW, it is often possible to instantaneously identify regions where high turbulence, or gradients of V and Z are most likely to exist without having to perform the traditional processing of the Z and V field data. Unfortunately, while these various factors are well known, little effort has been directed to clarify the true utility of SPW in feature identification and forecasting. This is the primary interest here.

2 METHODOLOGIES

The primary effort this first year focused upon understanding the variability of the WSR-88D SPW estimates over a variety of geographical locations and radars. Data from three sites were used, including Melbourne FL (MLB) (3 days) , Dodge City, KA (DDC) (2 days), and Lubbock , TX (LBB) (1 day). These data periods all included severe weather events (e.g. hail, surface wind gusts, tornadoes, etc.). Occasionally, a cursory review of other data was made to confirm any unusual behavior observed on the target days. The primary areas of interest included:

1. Three-dimensional (3D) visualization of storm SPW and precipitation (Z) structures
2. Correlation of SPW with Z, V, and gradients of Z and V over storm regions
3. WSR-88D problem areas

These types of analyses have rarely been performed and thus are a natural starting point for understanding the association of SPW with storms. The 3D visualization allows simultaneous viewing of the various radar derived storm parameters in relation to one another throughout the storm volume and removes much of the uncertainty that traditional 2D analyses often engender. Combined with time monitoring one may potentially identify SPW signatures that may be useful as precursors to storm feature evolution. Correlation analysis of collocated SPW and other radar derived variables describe the general dependency of SPW upon radar measured storm parameters. This is particularly useful for clarifying the origins of the SPW values as primarily turbulent or shear based, and whether these sources may be identified by viewing Z or V structures alone. These analyses also serve a secondary role as methods for data quality assessment, by clarifying if unusual SPW observations are “artifacts” from contaminating factors (e.g. multi-trip, clutter, hardware). This is valuable information since the SPW is the most sensitive of the three basic radar measurements (Z, V, SPW) to system and low signal to noise ratio (SNR) problems, and one must be able to identify whether SPW features are real or fictitious.

The 3D analyses provide striking and sometimes unexpected clues to the development of SPW features, and their associations with storm elements. Storms from the full operational range (0 - 230 km) were utilized to observe if there are any obvious range

dependent effects upon the SPW measurements. This reflects a concern not only for the accuracy of mapping the multi-trip Doppler (V, SPW) data between the first (approximately 120 km) and second unambiguous Doppler ranges, but also for the stability of the hardware system over the full 230 km Doppler range. General trends for increasing SPW mean values beyond those expected from shear and turbulence contributions could indicate a hardware problem. The 3D visualization focused primarily upon the regions of moderate to high Z, and gradients of Z and V, since these generally define the important storm structural elements.

The analysis shows that a variety of 3D spatial distributions of SPW are often present, ranging from highly organized (Melbourne, Day 221 (e.g. MLB221)), to moderately organized (MLB246), and to broadly distributed (most others). Occasionally, significant data artifacts, both real and artificially enhanced (e.g. DDC and LBB 3-body scatter observations) are noted. Since the WSR-88D systems are under strict configuration control, it is expected that variability in observations between radars would be meteorological in origin, aside from significant local variability in the clutter returns. The MLB221 data generally contain the greatest amount of clutter return within 10 km of the radar, with the coastline often clearly visible. Other MLB observations, however, do not display similarly large areas of significant clutter return. It is certainly possible that the refractive indices of air and ground objects varied significantly between observations. However, the existence of known MLB hardware problems, combined with the different behavior of the clutter and SPW data on MLB221, suggests a more variable hardware setup may have been in use at MLB.

The range of SPW estimates is occasionally within 0 - 8 m/s, generally within 0 - 12 m/s, and occasionally SPW exceeds 16 m/s. Values greater than about 6 m/s from research weather radars are typically considered large, and the continual presence of values greater than 8 m/s gives some cause for concern. This variability, whether real or not, forces the analysis of SPW data to be undertaken in two directions. The first is to quantify the magnitude and sources (e.g. dependency on Z, V, etc.) of SPW variability. The second is to identify the primary SPW patterns or structures associated with individual storms.

The MLB221 data present an interesting case and demonstrate some of the uncertainties that one faces when employing SPW data. The MLB221 data contain the greatest proportion of high SPW values observed within individual storms (Figures 1a-e) and

the most striking degree of organization for the precipitation (Z) and SPW structures. Individual storms are generally organized in groups along short lines, have nearly identical 3D structure, reach 10-11 km in altitude, and exhibit a maximum Z just above 60 dBZ. The individual storm groups contain either separated individual cells, or an elongated cell structure apparently formed from the merging of nearby cells. All cells exhibit a pronounced tilt in the direction of storm motion, presumably in response to the environmental wind shear. For those storm groups containing discrete cells, the 3D Z and SPW structures form distinct semicircular arc echoes of high Z (> 50 dBZ) and SPW (> 10 m/s) (Figure 1c) near storm midlevels (3-7 km), adjacent to the inferred updrafts. The rotation of the isocontours between midlevels and ground follows the rotating environmental wind direction. This unusual organization is repeated among many storm groups observed this day. It is suggestive of precipitation growth within the updraft, an accumulation of heavy precipitation (large drops and small hail) along the updraft boundary at storm midlevels, and then the return to ground along a circuitous path controlled by the environmental wind. Figure 1e, an expanded view of one cell region, shows the updraft column ($V = 0$ m/s, light isosurface) extending from near ground up into the midlevel arc region ($Z > 50$ dBZ, dark isosurface). Monitoring these structures over time suggests that the development of high SPW aloft precedes the development of the nearly collocated high Z structures.

These observations suggest that exaggerated SPW structures aloft may be precursors for accompanying precipitation development, a “signature” that may offer forecasting capability. However, the behavior of the SPW data on this day is quite different from that of other data sets, and thus the validity of the SPW data must be challenged. Reasons for concern include the (1) magnitude of SPW is considerably larger than observed in other data, (2) high SPW values appear positively correlated with high Z, and (3) the clutter signal is greater in magnitude and spatial extent than observed with the other two MLB periods analyzed. A reanalysis was performed with additional data quality processing to remove potentially contaminated data that could result from the incorrect activation of clutter filters during midlevel scans. This required eliminating sample volume data where V was within the range of about ± 6 m/s. The overall appearance of the MLB221 observations remain unchanged, with the high SPW values and striking 3D structures still retained. To identify

Reflectivity Factor & Surface Z 1992-03-26
02:36:22

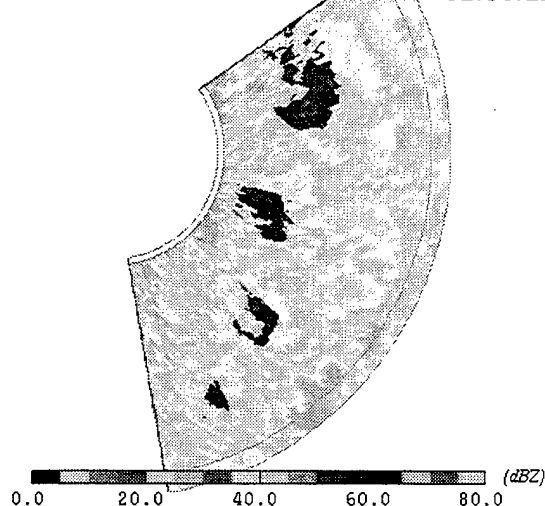


Figure 1a

Spectrum Width & Surface Z 1992-03-26
02:36:22

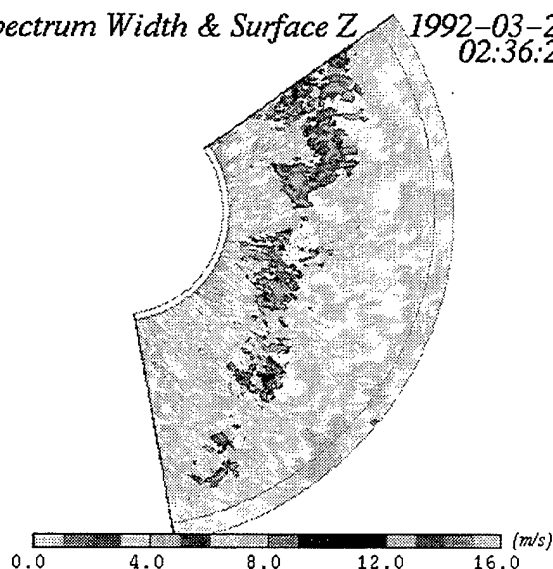


Figure 1c

Isosurfaces of V (.1m/s) & Z (53 dBZ)

1992-03-26
02:36:22

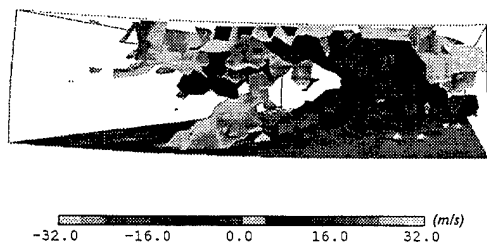


Figure 1e

Reflectivity Factor & Surface Z 1992-03-26
02:36:22

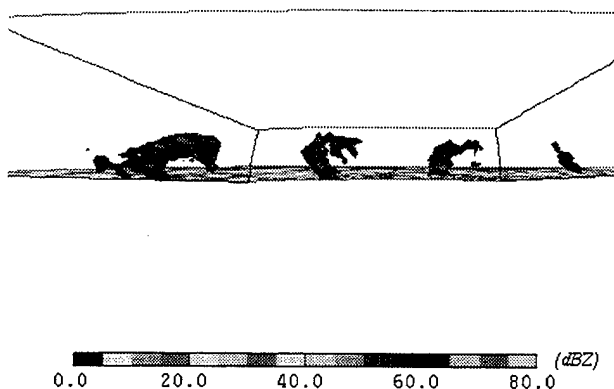


Figure 1b

Spectrum Width & Surface Z 1992-03-26
02:36:22

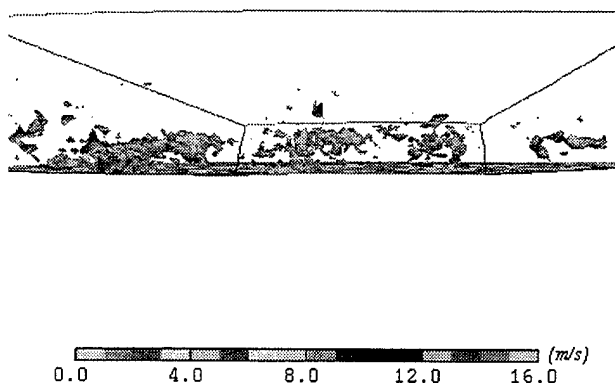


Figure 1d

Figures 1a-e. Highly organized 3D structures observed with Melbourne, FL WSR-88D on 03/26/92 (MLB221). Isosurfaces shown are for Z (50 dBZ) and SPW (12 m/s) overlaid onto surface scan Z field. Views from above show the striking curved structures in Z (a) and SPW (c). Side views (b, d looking from NW) show the arc structures are located at storm midlevels. Side view (e) from SE shows updraft ($V = 0$ m/s isosurface, light) rising into midlevel Z arc (50 dBZ, dark) for one storm. Descent of precipitation (Z) to ground follows rotation of wind direction through storm levels.

the origins of these very large SPW values, analyses of the various (radial, azimuthal, elevational) gradients of Z and V were performed. However, their contributions to SPW are not found sufficient to generate the total observed SPW. It is conceivable that significant turbulence exists near storm midlevels that could generate the observed SPW structures. However, the V shear contributions are already quite large and a comparable turbulence contribution would only increase the SPW by roughly 50%, to a total of about 9 m/s. This value is much less than the higher SPW values observed this day and one must conclude that the MLB221 SPW data are being strongly influenced by an unidentified system problem.

In contrast to these observations the MLB246/247, DDC and LBB data display a markedly less distinct organization of Z and SPW structures within the storm "interiors". The MLB247 (Figures 2a-c) data contain a series of small, intense storms that appear to develop in response to the dissipation of neighboring storms. The central precipitation core in the storm shown exceeds 50 dBZ and resides within a region of strong shear of the horizontal wind, apparently generated through the interaction of a broad updraft sitting above a rear inflow region (Figure 2c). The SPW isocontours clearly indicate that SPW is concentrated into two primary regions; (1) along the storm boundary near the rear inflow, and (2) near the outer edge of the updraft (inferred), extending into the anvil region. With dissipation, the precipitation core settles towards the ground and is accompanied by a region of high SPW within and just downwind of the core. This is likely a region of strong shear or turbulence at the surface just ahead of the storm. The complexity of the SPW field structures do appear to vary with degree of storm maturity.

The MLB246 data (Figures 3a,b) include a number of small storms, some of which produced hail. They are smaller in volume and maximum Z than the DDC and LBB storms that also produced significant hail. Figure 3a indicates that only one storm has any sizable precipitation core (40 dBZ) region at this time. There appears to be no significant SPW (Figure 3b) associated with this precipitation core (Z), the single isocontour shown (6 m/s) actually lies between this storm and a smaller dissipating storm to the west (barely detectable Z isocontour near ground at left). Also worthy of note is the ring of high SPW located at the Doppler unambiguous range, an artifact generated by the WSR-88D system.

The Dodge City data includes two storms, a large single-cell storm northwest of the

Reflectivity Factor

1992-05-28

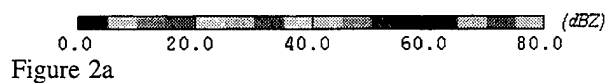
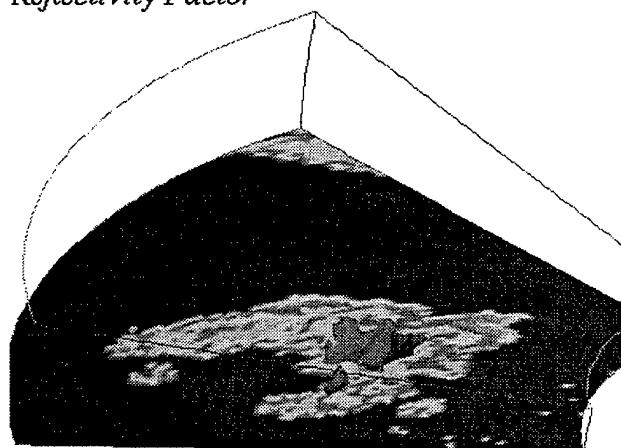


Figure 2a

Spectrum Width

1992-05-28

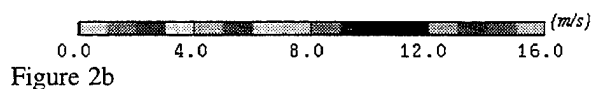
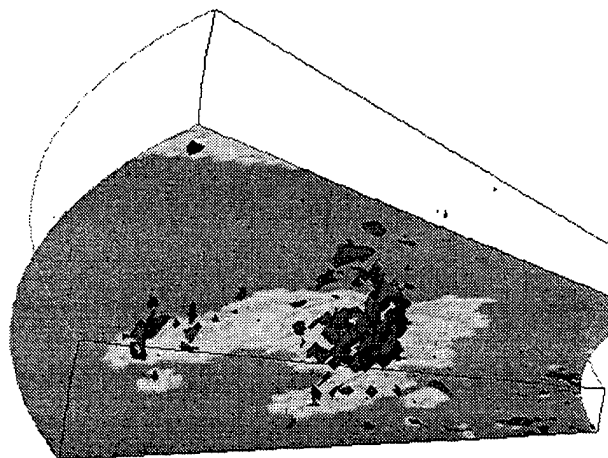


Figure 2b

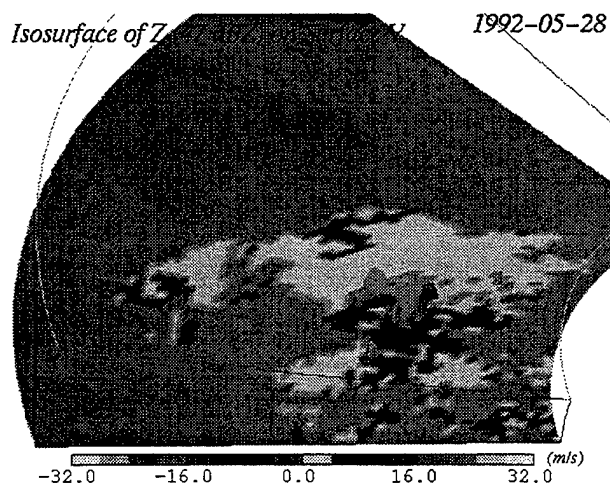


Figure 2c

Figures 2a-c. Moderately organized 3D structures observed with Melbourne, FL WSR-88D on 05/28/92 (MLB247). Isosurfaces shown are for (a) Z (45 dBZ) and (b) SPW (5.5 m/s) overlaid onto surface scan Z field. Views from SW show some correlation between Z and SPW structures. Z isosurface on V surface scan (c) shows Z cell lies adjacent to inflow (dark area to right) and above downdraft (dark area beneath and to left) airflows. Note moderate SPW resides throughout storm volume to greater extent than Z.

radar, and a two-celled structure to the northeast. Both exhibit core regions of no distinctive form, particularly for the northeast storm that is well in decay. The northwest storm core (> 50 dBZ isocontour) is extensive in volume and “lumpy” in appearance. Isosurfaces at moderate Z (25 - 40 dBZ) are equally nondistinctive. The SPW data reach moderately high values (0 - 12 m/s) and show no distinctive large scale organization “within” the storms.

Figure 4 (DDC) shows that high SPW exists on the “periphery” of the 40 dBZ storm precipitation volume. The mean SPW found within the storm boundary ($Z = 5 - 15$ dBZ) generally increases with increasing elevation (also observed in the MLB data), suggesting increased contribution from wind shear and turbulence at higher storm levels. The increased contribution from viewing falling precipitation at greater elevation angles should be quite secondary. These various data sets indicate a wide variability in the SPW structure may be expected between storms, and within individual storms as they evolve over time.

The DDC data show some highly distinctive SPW structures are found to be associated, but not collocated, with the dominant Z features found within storms. These are found (1) adjacent and behind the highest Z (GE 55 dBZ), (2) extending outside the storm boundary at similar range, and (3) lying above the core and near storm top (5-15 dBZ) level. While some of these features are likely “artifacts” rather than of meteorological origin, they do suggest that organized regions of high SPW are likely to be found near storm boundaries.

The observation of high SPW near storm top likely reflects a combination of high levels of turbulence and weak return signals that just exceed data quality (e.g. SNR) thresholds. Located within the anvil region, they often appear more broken than the 3D regions at lower storm altitudes. Combined with the observation that they are more prevalent at close range strengthens the argument that noisy, weak (low SNR) signals may be a significant source of high SPW in this storm region.

The “azimuthal” extensions of high SPW beyond radar storm boundary ($Z=5-15$ dBZ) at similar ranges to storm cores ($Z > 60$ dBZ) clearly result from radar beam sidelobe contamination generating spurious SPW estimates where no storm data really exist. Here, these extensions are generally observed on the southern side of the storms, reflecting the preferential placement of the high precipitation cores within the storm volumes. Sidelobe extension into the storm interior does exist, but it is masked by the higher return from the

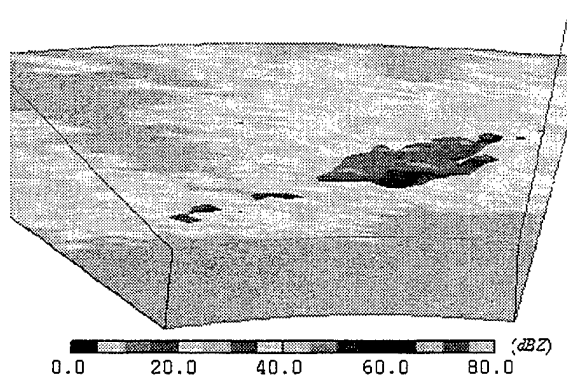


Figure 3a

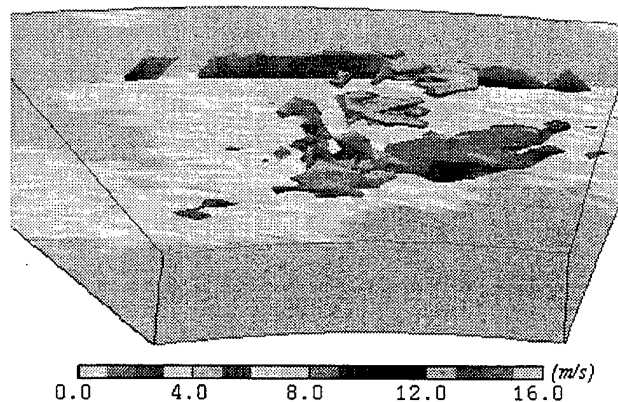


Figure 3b

Figures 3a,b. 3D structures observed with Melbourne, FL WSR-88D on 05/26/92 (MLB246). Displays show 3D isosurfaces for (a) Z (45 dBZ) for active storm (center right) and dissipated storm (small isosurfaces to left) along with (b) Z and SPW (7 m/s) overlaid onto surface scan Z field. Views from S show little correlation between Z and SPW structures at these thresholds with SPW actually lying between the two storms.

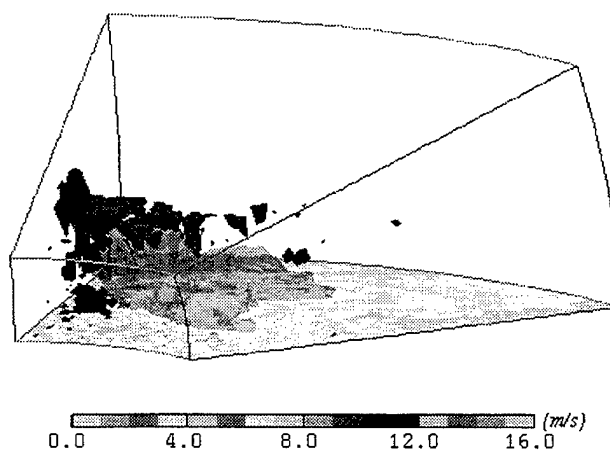


Figure 4. 3D structures observed with Dodge City, KA WSR-88D on 05/16/95 (DDC). Shown are 3D isosurfaces for (a) Z (40 dBZ, light) and (b) SPW (9.5 m/s, dark) overlaid onto surface scan Z field. View from E shows little correlation between Z and SPW structures at these thresholds with largest regions of high SPW lying above, aside, and behind storm precipitation core.

storm precipitation found there. These extensions are best noted in the SPW data because these SPW values are noticeably higher than generally found along the radar storm boundary, while the accompanying Z extensions are of low intensity and can be easily mistaken as part of the normal boundary. The WSR-88D data quality thresholding process generally removes artifacts along storm boundaries by thresholding out signals of insufficient returned power (low SNR).

Of considerable interest are the extended regions of low Z (< 15 dBZ) and high SPW (> 8 m/s) located "behind" the high Z (> 62 dBZ) cores, extending outside the storm boundary. This phenomenon appears behind precipitation cores of Z exceeding about 62 dBZ. Figures 5a-d show such extensions covering a 2-5 degree azimuthal swath and extending a few km out beyond the gently curved storm boundary.

These features are most notable at storm midlevels, and in 3D visualization appear as "bumps or spikes" on the storm rear boundary isosurfaces ($Z \leq 15$ dBZ). A second example is shown in the LBB data (Figures 6a-d) where narrow (1-2 degrees) extensions extend many km into the "clear air" behind the storm core.

Both observations are likely due to "3-body" scattering, an infrequently observed phenomenon that typically occurs only when large hail is present (Zrnic, 1987, Wilson and Reum, 1986). Because of the large hail size, the power scattered towards the ground and subsequently scattered back to the hail region, and then back to the radar is sufficient to be detectable. The additional scattering from the ground and hail region alters the phase of the signal received at the radar receiver, resulting in increased values of SPW. In both the DDC and LBB cases, the 3-body signature is most easily identified in the SPW data since the high SPW values within the spike are generally very distinct from those along the adjacent storm boundary, while the low Z values in the spike are similar to those along the storm boundary.

It is curious that the SPW and Z spikes are of equal length for the DDC storm (Figure 5), whereas for the LBB storm (Figure 6) the SPW extension is about twice as long. Ideally, one expects the Z/SPW extensions to be similar in length (depending upon SNR thresholding) and about twice the height of the hail scatter region (if small) above ground on the current elevation scan. For DDC the Z and SPW extensions are about 6-10 km in length,

Reflectivity Factor

1995-05-16
23:02:53

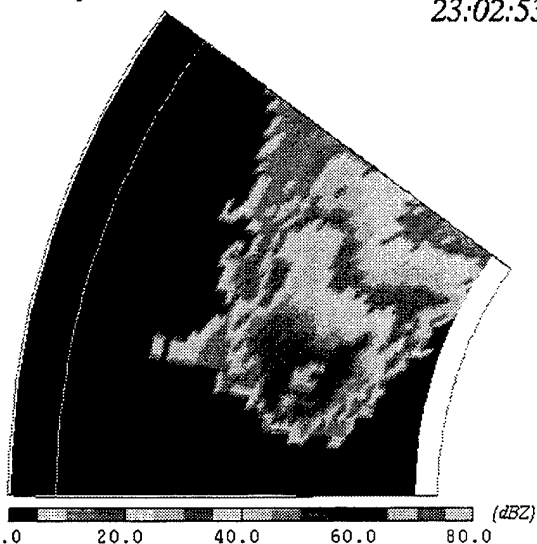


Figure 5a

Spectrum Width

1995-05-16
23:02:53

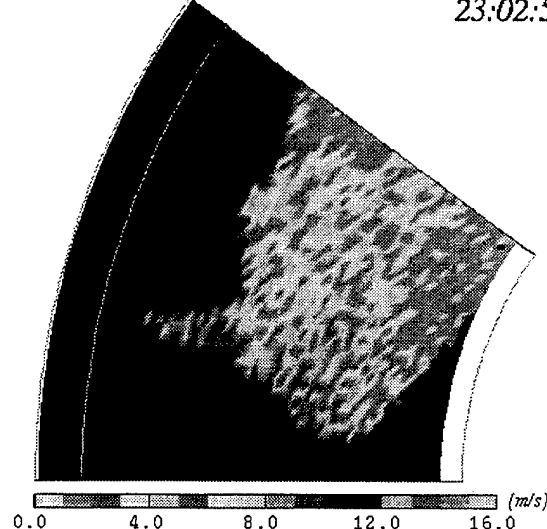


Figure 5b

Isosurface of Z on Z (scan 5)

1995-05-16
22:51:47

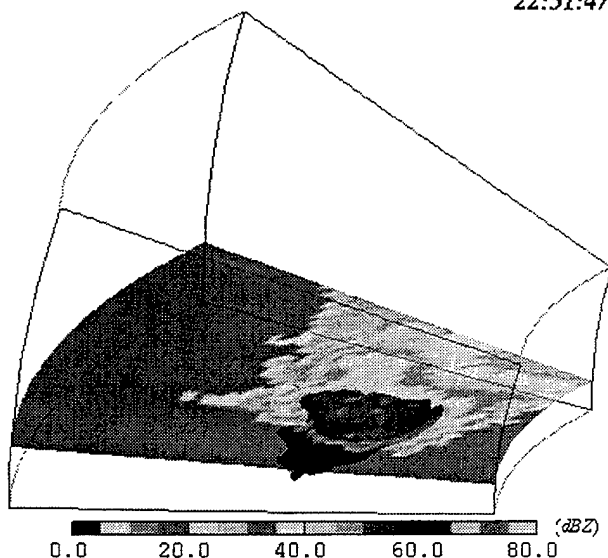


Figure 5c

Isosurface of SPW on SPW (scan 5)

1995-05-16
23:02:53

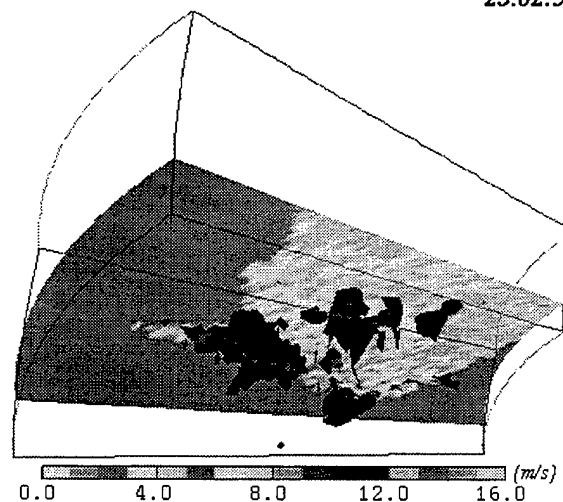


Figure 5d

Figures 5a-d. Displays of 3-body scatter signatures from Dodge City, KA WSR-88D on 05/16/95(DDC). Spikes behind storm core at midlevels seen in fifth elevation scan for (a) Z and (b) SPW, and in 3D views from S showing 3D (c) Z and (d) SPW structures. Extension of SPW isosurface along spike (Z isosurface limited by WSR-88D color display scheme) demonstrates how high SPW and low Z values make SPW easier to detect. Feature should not be mistaken for "normal" storm boundary due to (a) moderately narrow (3-4 radials) extensions for Z and SPW, (b) location radially behind precipitation core, and (c) combination of low Z and heightened SPW.

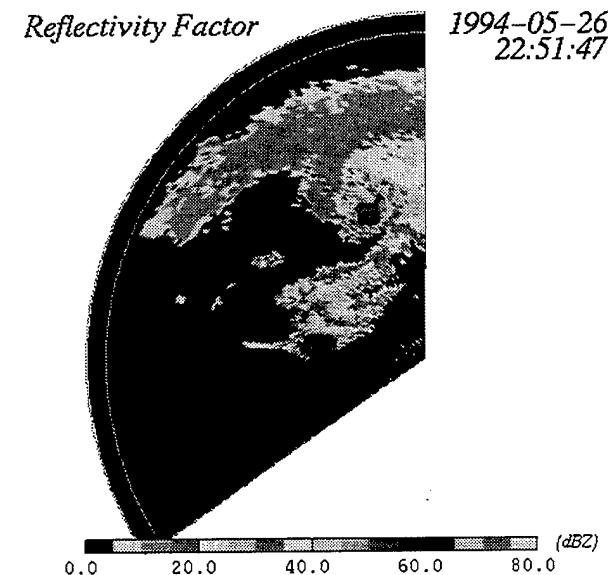


Figure 6a

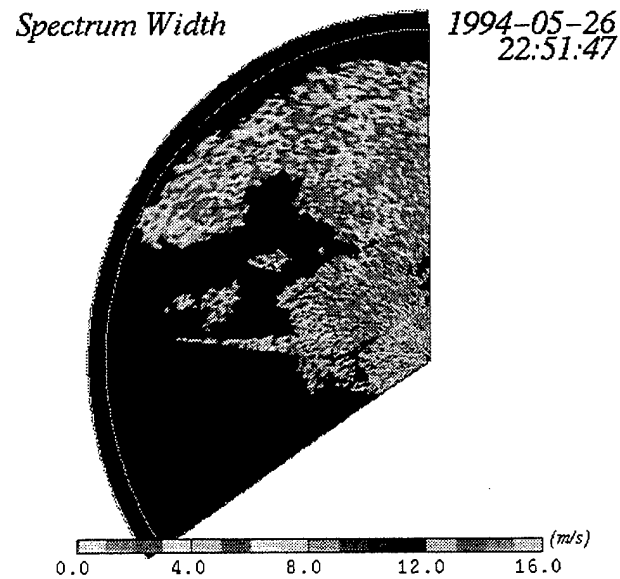


Figure 6b

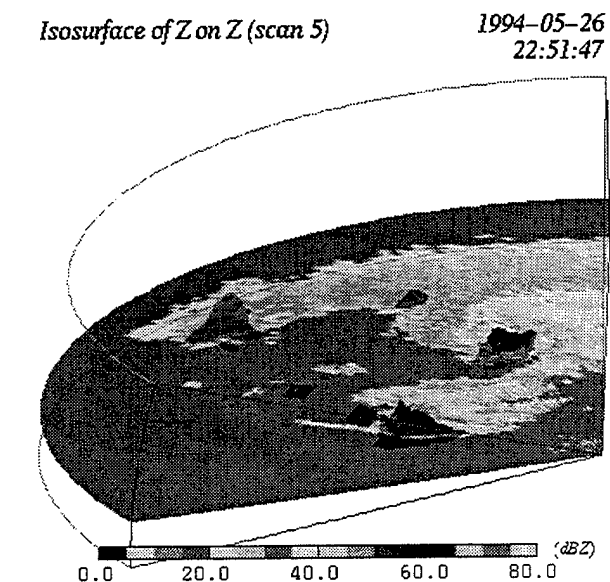


Figure 6c

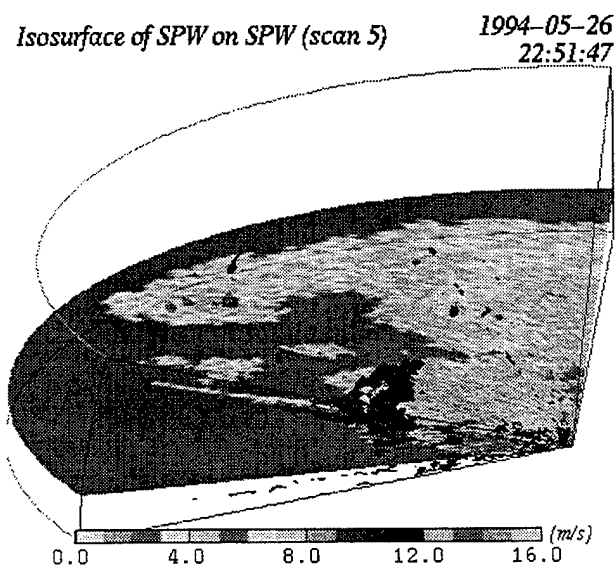


Figure 6d

Figures 6a-d. Displays of 3-body scatter signatures from Lubbock, TX WSR-88D on 05/26/94 (LBB). Spikes behind storm core at midlevels seen in fifth elevation scan for (a) Z and (b) SPW, and in 3D views from S showing 3D (c) Z and (d) SPW structures. Extension of SPW isosurface along spike (Z isosurface limited by WSR-88D color display scheme) demonstrates how high SPW and low Z values make SPW easier to detect. Feature should not be mistaken for "normal" storm boundary due to (a) striking narrow (1-2 radials) extensions of 9 and 20 km for Z and SPW, (b) location radially behind precipitation core, and (c) combination of low Z and heightened SPW values.

in reasonable agreement with an altitude of 3-4 km for the high Z (> 64 dBZ) region. For LBB, however, the precipitation core maximum is about 4 km above ground and the Z and SPW spikes are about 9 km (reasonable) and 20 km (unreasonable) in length, respectively.

Use of different SNR thresholds on the Z and V/SPW data channels may be partly responsible for length differences, or the V/SPW data channel may have become saturated from the large power impulse received directly from the hail region. Failure of this channel to stabilize quickly could generate large SPW values for following range gates. Alternatively, the discrepancy may be an artifact of the WSR-88D color "display" scheme thresholding out some data. While this 3-body signature was occasionally observed in DDC and LBB data, only one suspected event was noted in MLB data, perhaps reflecting the smaller hail ($Z < 64$ dBZ) found there. These results suggest that WSR-88D SPW may be quite useful in detecting the presence of the elusive 3-body scatter signature associated with large hail.

Other potentially hazardous features may also be observed via the SPW. It was occasionally noted that shallow wind shift features (e.g. gust, pre-frontal) can be detected in these data. These flows are generally of low Z value, and include a significant amount of wind shear and turbulence near the wind shift zone. Often, however, the narrow width of these features precludes standard wind shear estimation and detection since velocities from forward and rear sample gates may not be available. Thus, SPW, available on a sample volume scale, may be highly supportive in detecting these features. As an example, the MLB221 data contain a shallow gust front ahead of an advancing storm group. It lies just within the radar storm boundary and is less than 1 km deep. A Z signature (Figure 7a) is not observed for any Z threshold. However, the SPW signature (Figure 7b) is clearly seen ahead of the precipitation core just inside the radar storm boundary.

Similarly, Figures 8a-d display a wind shift feature that is only suggested in the Z (Figure 8a) data, quite easily observed within the V (Figure 8b) and SPW (Figure 8c) data, and not observed at all in the 2D V gradient data (Figure 8d). The 2D shear estimate fails here because the width of the wind shift line is too narrow to support the 3-point algorithm used in gradient estimation. Alternatively, Figures 9a-c clearly show a distinct boundary layer Z "thin line" ahead of an approaching cold front. In this instance, only a small portion of this line feature is detected within the V and SPW fields. With the Z values (5 - 10 dBZ) and

ranges similar for all three cases, the variability in detectability between the three data elements Z/V/SPW suggests that different data thresholds (e.g. SNR) are being applied to the Z/V channels for the two radars. These examples demonstrate that SPW can be highly useful in detecting shallow wind shear zones, but only if the SNR thresholds are appropriately set.

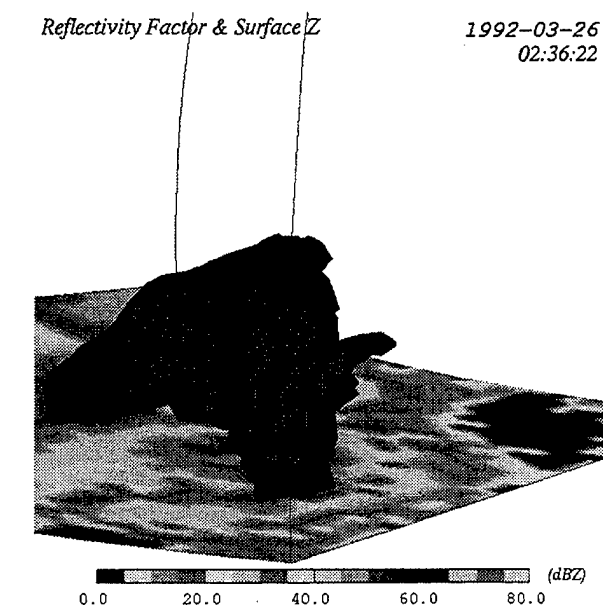


Figure 7a

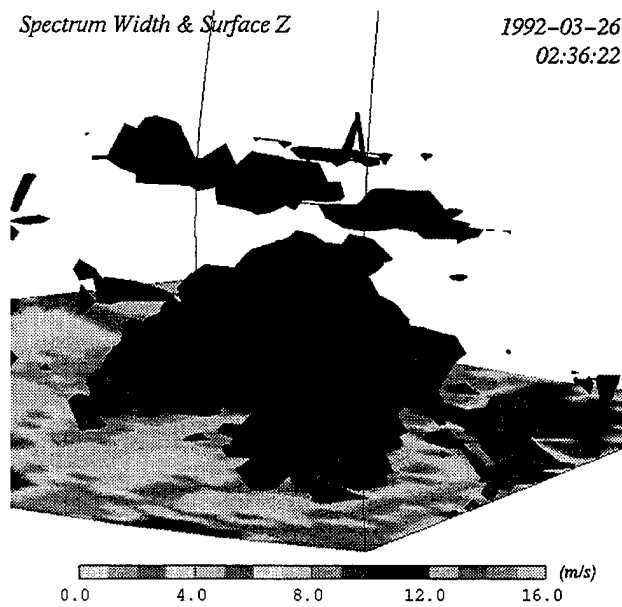


Figure 7b

Figures 7a,b. 3D displays of Z and SPW isosurfaces overlaid onto surface scan Z fields for large storm NW of Melbourne, FL WSR-88D on 03/26/92 (MLB221). View from SW shows precipitation core of 50 dBZ leaning downwind with increasing height with no low level Z feature observed (for any Z) ahead of storm (to right). Shallow SPW structure of high value (10 m/s) is observed at surface, outside storm boundary, and ahead of the main SPW and Z structures. Note that the high SPW associated with storm core is likely hardware enhanced, but windshift line is likely not hardware enhanced due to low Z (power) there.

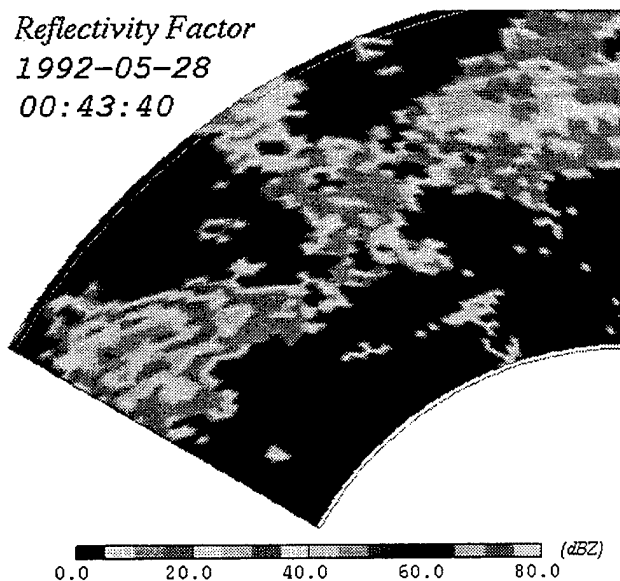


Figure 8a

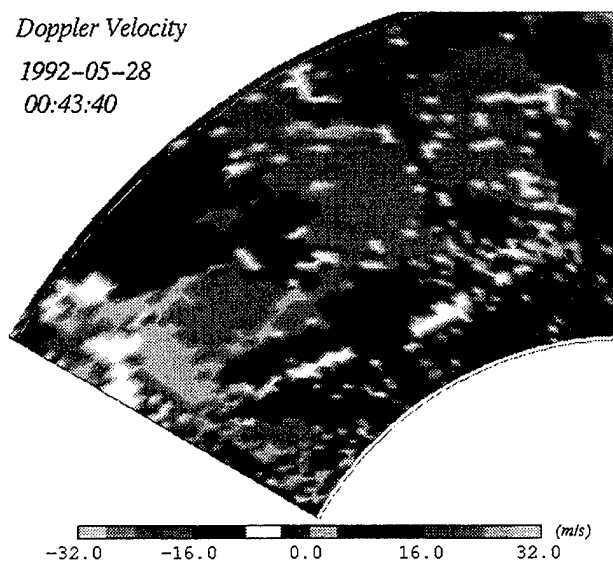


Figure 8b

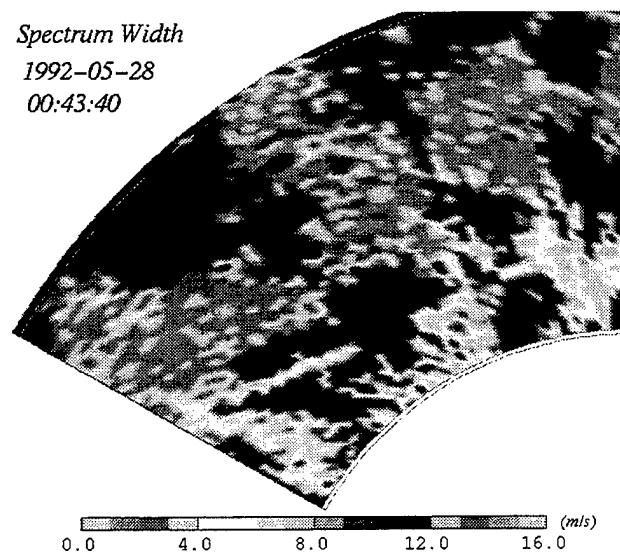


Figure 8c

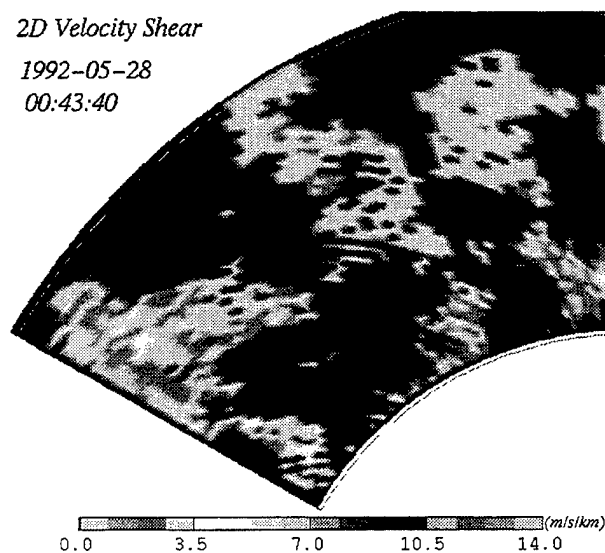


Figure 8d

Figures 8-a. 2D displays of Z, V, SPW and 2D velocity shear on surface scan indicating detectability of surface gust front (line oriented SW-NE) in lower center) located in clear air ahead of storm complex. Line is poorly observed in (a) Z, but well detected in (b) V and (c) SPW. Line is not well detected in (d) 2D shear field due to narrowness (often 1 sample volume deep (1 km resolution)) of feature and 3X3 gradient template. Data are from Melbourne, FL WSR-88D on 05/26/1992 (MLB246).

Reflectivity Factor 05-23-1993

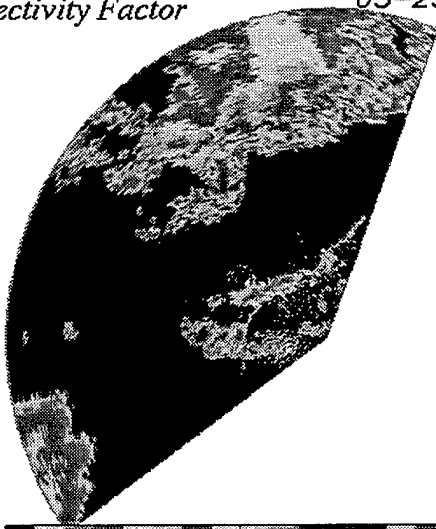


Figure 9a

Radial Velocity 05-23-1993



Figure 9b

Spectrum Width 05-23-1993

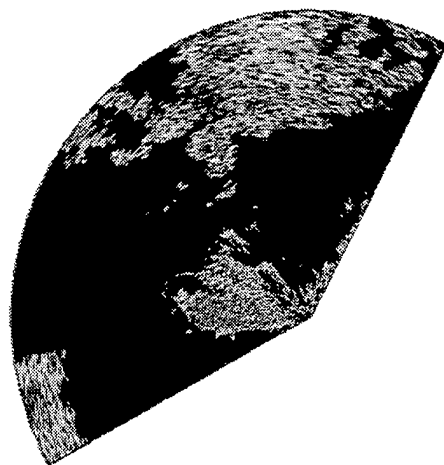


Figure 9c

Figures 9a-c. 2D displays of Z, V, and SPW on surface scan indicating detectability of surface gust front (SW-NE line near radar) located in clear air ahead of storm complex (also oriented SW-NE). Line feature is well observed in (a) Z, but poorly detected in (b) V and (c) SPW due to decreased areal coverage resulting from Z and V/SPW data quality thresholding. Data are from Dodge City, KA WSR-88D on 05/23/1993.

3 CORRELATION OF SPW AND COLLOCATED Z AND V

Correlating SPW with collocated Z, V, and their respective gradients can be quite useful in assessing the origins and overall characteristics of the SPW throughout the target storms. Correlating Z with SPW should provide some identification of the degree of organizational dependence of Z with the local wind shears. In simple cellular storms this dependence may be high, whereas with large organized storms generating large amounts of precipitation over wide spatial volumes, this association may be low. Surprisingly, the Z-SPW correlation is found to provide some insight into the issue of SPW data quality.

Correlating V and SPW is less successful since the observed Doppler velocity is dependent upon both the wind and radar viewing directions. Generally, SPW is found uniformly distributed with V. If any strong correlation is indicated, it likely reflects a fortuitous chance of alignment of wind direction along the radar viewing direction to the storm. More meaningful are the correlations of SPW with the V shears, although these measurements also suffer from angle dependency. Nonetheless, there is a potential for qualitative assessment of the relative contributions of turbulence versus velocity shear to SPW. To date, in this study most correlations have been made against Z, but future efforts will provide greater focus on V shears, and turbulence.

While the “shape” of the Z-SPW distributions may evolve with time, they may be classified in terms of their “uniformity” and the presence/absence of “SPW tails” at low and high values of Z. A uniform distribution indicates that SPW and Z are not well correlated, and thus a given value (low, moderate, high) of SPW is equally likely to be found in regions of low, moderate, and high Z. The MLB247 (Figure 10) storms exhibit this distribution shape. By comparison with most other storms analyzed here, this distribution is extremely narrow in SPW range, being only 0 - 8 m/s in width. The DDC and LBB storm distributions are occasionally uniform, but with a larger range of SPW values (0 - 12 m/s). In 3D visualization, the storms that generate this distribution form generally display little sidelobe, storm boundary, hail scattering, or multi-trip contamination in the SPW data fields.

Distributions with a single SPW tail at low values of Z are generally observed. The

Spectrum Width vs Reflectivity Factor

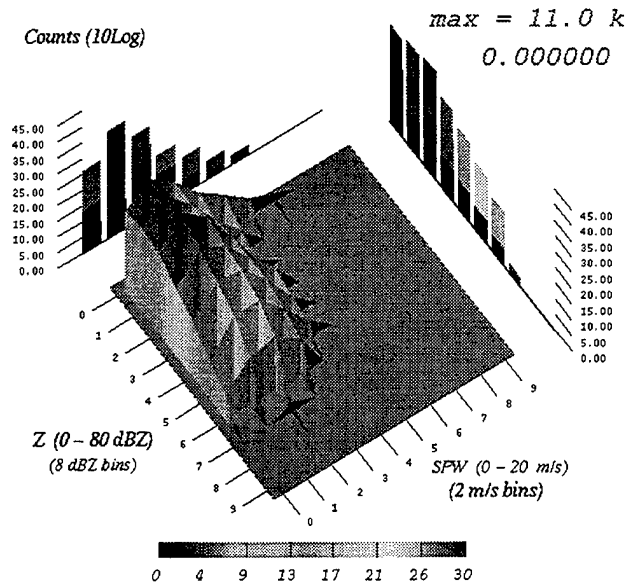


Figure 10. Example of uniform correlation distribution between collocated SPW and Z for storm observed by Melbourne, FL WSR-88D on 05/27/92. Maximum Z generally less than 56 dBZ and little SPW is observed above 8 m/s. Little clutter or other data contamination effects are observed in these data. Format: SPW increases to right, Z increases from the left. Numbers per bin displayed along vertical axis as 10LOG(number).

range of SPW is broad (0 - 20 m/s) at the lowest values of Z (5 - 24 dBZ), with the spread of SPW values quickly decreasing at higher values of Z. The DDC frontal case (Figure 11) and LBB (Figure 12) data are representative of this situation. This correlation between high SPW and low Z likely reflects both (1) contaminated data associated with storm boundary, multi-trip, and clutter regions where data perhaps just exceed SNR data quality thresholds, and (2) the regions of high SPW near storm periphery that are associated with hail spikes and inflow regions. This association is most frequently observed with the larger storms and the counts per bin within the SPW tail appears to generally decrease with decreasing storm size “as viewed by the radar”. This reinforces the notion that the tail is often dominated by samples from storm boundary regions. Thus, this relationship to “radar storm size” may simply reflect the smaller number of radar sample volumes required for viewing the boundaries of smaller storms, or when monitoring individual storms moving to greater range.

Spectrum Width vs Reflectivity Factor

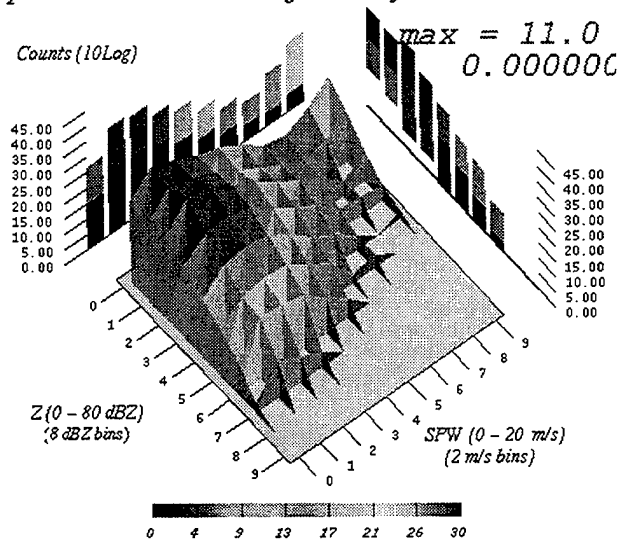


Figure 11a

Spectrum Width vs Doppler Velocity

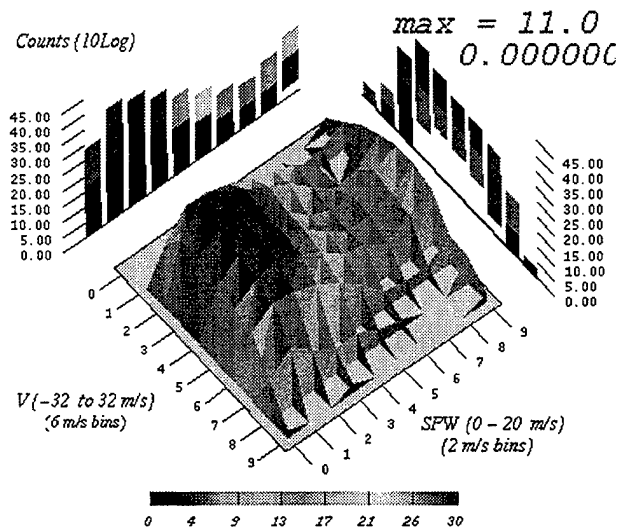


Figure 11b

Figures 11a,b. Example of unusually broad single-tailed correlation distribution between collocated SPW and (a) Z and (b) V for storm observed by Dodge City, KA WSR-88D on 05/16/95. Format same as Fig.10. Z ranges from 0 -> 64 dBZ, with SPW between 0 - 20 m/s in tail region and 0 - 16 m/s elsewhere. Marked distinction of lower tail from rest of distribution is not readily observed. Fig. 11b shows increasing SPW correlated with decreasing V range, but no preference for +V vs -V values. Note, results using V dependent upon wind and radar viewing directions. Increased SPW contributions at 18-20 m/s bin are likely an artifact of WSR-88D processing.

In 3D visualization, storms associated with this distribution feature generally have easily detectable sidelobe, storm boundary, or multi-trip effects. By observing the proportion of data falling into this lower tail one can gage the relative degree of difficulty these data would present to automated analysis, with a greater likelihood for false alarms associated with a greater proportion of observations falling into this tail region. Figure 11b shows the correlation between V and SPW for this DDC cold front case. Over a wide viewing volume V and SPW typically appear uncorrelated. This is not surprising since SPW responds to the V shear, not the value of V itself. Here there is a slight preference for increasing SPW to be associated with a decreasing range (+/- about 0 m/s) of velocities.

Another interesting case is the double-tailed distribution, where the breadth of SPW values is greatest at both the lower and higher Z bounds. Assuming the lower tail represents

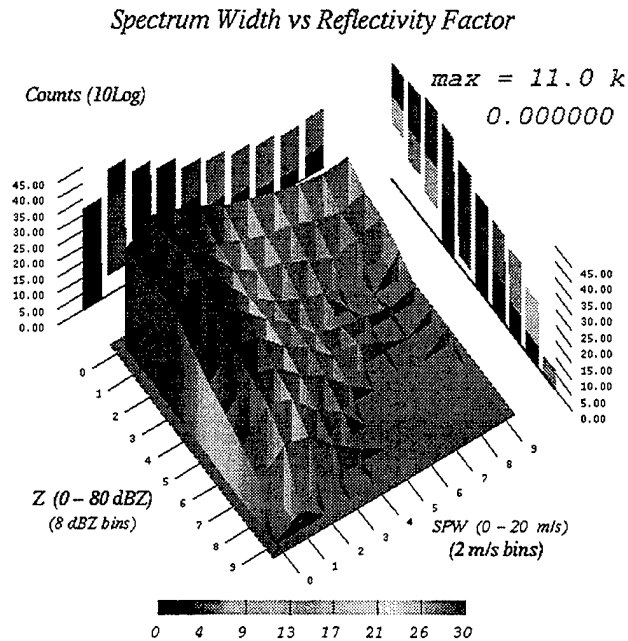


Figure 12. Example of single-tailed correlation distribution between collocated SPW and Z for storm observed by Lubbock, TX WSR-88D on 05/26/94. Format same as Fig. 10. Z ranges from 0 -> 72 dBZ, with SPW between 0 - 20 m/s in tail region and 0 - 12 m/s elsewhere. In this example, distinction of lower tail from general distribution readily observed. Here, all very high SPW generally occurs with Z < 25 dBZ, associated with storm boundary regions and clutter.

storm periphery data, the correlation with high values of Z would be expected to reflect the contributions from turbulence and gradients of Z and V that often accompany the more intense (e.g. greater Z) storm regions. The DDC (Figure 13) data show a typical double-tail distribution containing significant amounts of data at low Z and a general broadening of the SPW range above 40 dBZ. At this time the storm is large in volume with a maximum Z approaching 72 dBZ. The MLB246 data (Figure 14) show a similar distribution shape for a small storm reaching only 56 dBZ. Here the small upper tail begins to form near 32 dBZ. By generating Z-SPW distributions from data within narrow altitude layers, it was found that the primary source regions for the upper tail often lie near and above the storm midlevels (5-7 km for MLB221, 4-10 km for DDC, and 5-11 km for LBB).

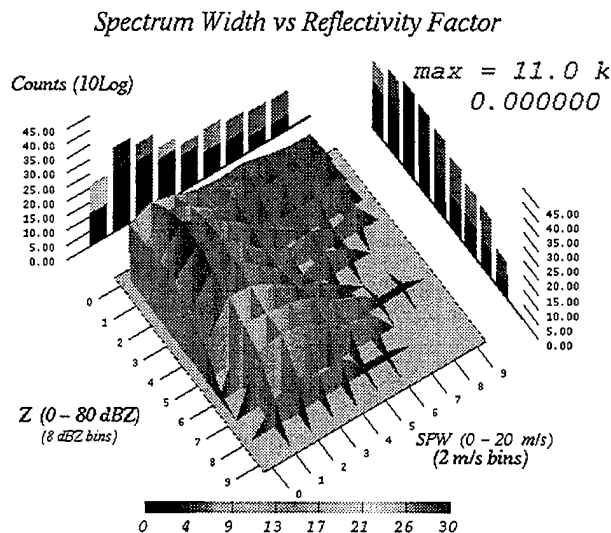


Figure 13. Example of double-tailed correlation distribution between collocated SPW and Z from Dodge City, KA WSR-88D on 05/16/95. Format same as Fig. 10. Z ranges from 0 - 72 dBZ, SPW from 0 - 18 m/s in lower tail and 0 - 14 m/s elsewhere. Note that minimum SPW values in upper tail (Z GE 48 dBZ) are shifted above 0 m/s and the range of SPW values has increased.

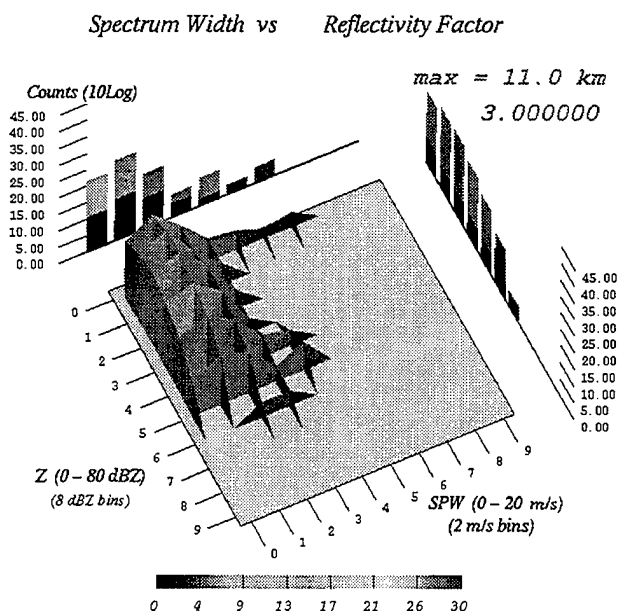


Figure 14. Example of double-tailed correlation distribution between collocated SPW and Z from Melbourne, FL WSR-88D on 05/27/92 (MLB246). Format same as Fig. 10. Z ranges from 0 - 48 dBZ, SPW from 0 - 8 m/s below upper tail and 0 - 10 m/s within upper tail.

The upper tail is usually (1) broad (e.g. 0 - 12 m/s wide), (2) not usually associated with Z below 40 dBZ, and (3) has a lower bound displaced (minimum SPW) towards higher SPW. Thus, while the lower tail appears anchored to SPW = 0 m/s, the upper tail is often separated from it. It must be noted, however, that high values of Z do not demand the presence of this upper tail, since other DDC (Figure 15) and LBB (Figure 12) data periods with Z exceeding 72 dBZ show no SPW broadening whatsoever. It is suspected that the upper tail reflects a higher degree of organization in the precipitation and wind fields and it may be a method for identifying the presence of large wind shears when direct measurement is difficult.

However, an accentuated upper SPW tail may be a cause for concern. The most highly skewed double-tailed distribution is found in the MLB221 (Figure 16) data where the maximum Z is only near 64 dBZ. As previously noted, these SPW data are considered highly suspect. The Z-SPW distribution shows the upper tail to be very broad, and the minimum SPW value (lower bound) increases dramatically with increasing Z. In 3D visualization the high SPW regions are well collocated with the regions of high Z. Both are organized into very distinctive arc-shaped structures at storm midlevels that encircle the updraft (Figure 1e), and then spiral down towards the ground following the changing environmental wind direction. Because of the small size and strongly curved nature of these Z structures, it was originally believed that the combination of high Z gradients and close range could generate the very high SPW observed. This belief was strengthened after reprocessing the data to remove contaminated data samples resulted in only a proportionately decreased population number across the distribution with little effect upon distribution shape.

The MLB221 data were further analyzed to determine the origins of the SPW estimates by ascertaining the dependence of SPW upon various field gradients. Figures 17a-i show the correlation results with various gradients of Z and V in the radar (spherical) reference frame for a single storm approximately between 12 - 25 km range. Unlike the Z-SPW correlation distribution, there is no readily detectable dependence of SPW upon individual radial, azimuthal, or elevational gradients of Z (Figures 17a-c) nor with the 3D gradient of Z (Figure 17g). This is the first strong flag of concern since the local Z gradient, not the value of Z (Figure 16), should control any Z contribution to the SPW estimate. This suggests a possible system problem with this MLB221 data where received power above a threshold value may be corrupting the SPW estimates.

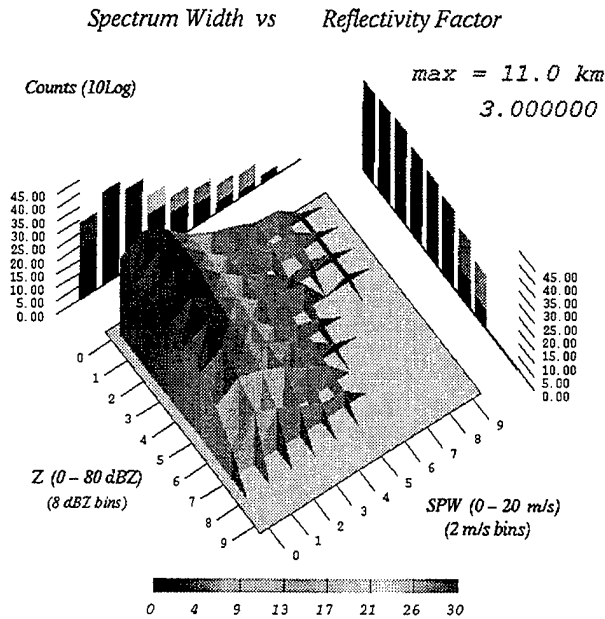


Figure 15. Example of near uniform correlation distribution between collocated SPW and Z from Dodge City, KA WSR-88D on 05/16/95. Format same as Fig. 10. Maximum Z is generally less than 80 dBZ and SPW is generally less than 8 m/s. Despite high Z observed, little clutter or other data contamination effects are observed (minor lower tail), along with no observed broadening at upper Z (upper tail) values.

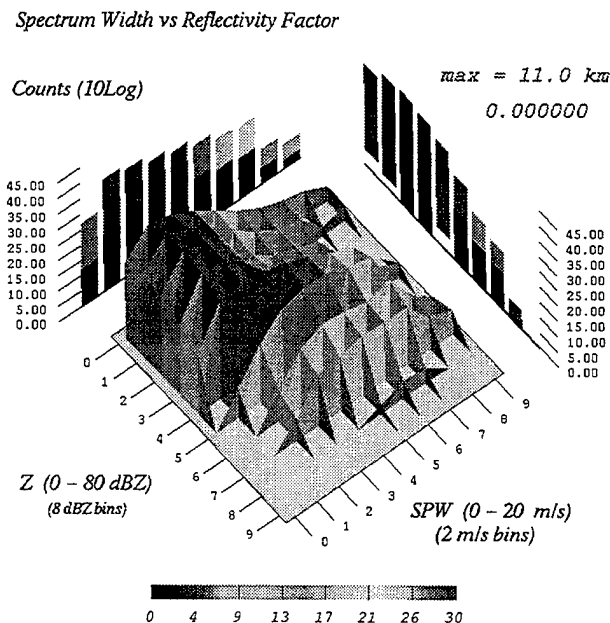


Figure 16. Example of exaggerated double tailed correlation distribution between collocated SPW and Z for Melbourne, FL on 03/26/92 (MLB221). Format same as Fig. 10. Upper tail displays significant shifts in SPW lower bound with increasing Z. General range of SPW values is extremely broad (0 - 16 m/s), extending to 0 - 20 m/s for Z between 32 - 40 dBZ. Exaggerated upper tail is likely enhanced by WSR-88D system problem.

While there does not appear to be any sizable correlation of SPW with individual 1D V gradients (Figures 17d-f), there is a strong correlation with the 3D gradient of V (Figure 17h). It is noted that within each Grad V interval above 20 m/s/km, the number/bin for SPW entries appears to increase slightly with increasing SPW, indicating a preference for higher SPW values to be associated with higher shears. More striking however, is the distinct increase in SPW lower bound with increasing Grad V. The contribution to SPW from Doppler velocity shear is estimated using the transverse shear relation of

$$SPW = .3KRT$$

where SPW is in m/s, K is the gradient in m/s/km, R the range in km, and T the full one way 3 dB beam width in radians. At a range R = 20 km and beamwidth of 1 degree, this relation is approximately $SPW = 0.1 K$. With a V gradient of 10 m/s/km, this implies a contribution to SPW of 1.0 m/s. Assuming the elevational shear and turbulence provide comparable contributions to SPW, we obtain an approximate maximum contribution to SPW of about

$$SPW = (.3KRT) \text{ SQRT}(3) = 0.17 K$$

for this example. Drawing a straight line through the "approximate" SPW lower bound locations suggests a dependence between SPW and the 3D V shear roughly equivalent to the relation above. Thus, it appears the "lower bound shift" may be equivalent to the potential contribution due to the large V shears. With the estimated 3D shear reaching over 50 m/s/km at this close range, a total contribution to SPW of 8 - 9 m/s is estimated. All remaining contributions from scanning, fallspeed effects, etc. would increase this by 1-2 m/s at most, providing a total contribution to SPW of 10 -11 m/s. This, however, is well below the observed maximum of near 20 m/s, leaving the origin of this high SPW unknown.

One may question the origin of the extreme V shear values noted here even though it is noted that the total number of sample volumes with such large shears are a small fraction of the total sample volume number included in this distribution. In 3D visualization the V data were observed to be very erratic near the precipitation cores at storm midlevels. This may be due to strong turbulence, an artifact generated by a system problem, or a combination of both. With sample volume separations of only 1/3 km, any large fluctuations present in the V data are magnified into very large shears. At greater range, these regions of large

fluctuations are subpulse volume in size and are averaged out and not often seen. Thus, while not generally expected, such large shears are possible when measured at short range. However, one must not forget that these large shears are derived from the “recorded” WSR-88D data, and need not mirror the actual environment if a system problem is affecting the data entering the receiver prior to downstream processing. Thus, if the V data and subsequent derived shears are not correct, there need not be a correlation between SPW and V gradients unless both V and SPW are simultaneously and similarly affected.

The final part of the puzzle is to determine if the large 3D V shear is correlated with high values of Z. Figure 17i indicates that a strong correlation does in fact exist between Z and the 3D shear of V, with the increasing 3D Grad V values existing primarily with increasing Z. Thus, the precipitation core, particularly the arc feature at storm midlevels contains very high Z values, is collocated with very high V shear and very high SPW values. The contributions from such large shear and turbulence have been shown sufficient to “increase” the SPW by values only equivalent to the lower bound shifts. Thus, one is tempted to assume that strong wind shears played a vital role in organizing the extraordinary arc structures observed here.

However, three elements are yet not explained. First, it is not “necessary” that large 3D shear be predominantly collocated with high Z precipitation structures. Second, while the largest shear and turbulence contributions can generate a contribution to SPW “equivalent” to the lower bound shift, these contributions should control the SPW “upper bound” values and not the lower bound shift, and thus the full expanse of SPW values approaching 20 m/s cannot be explained. Third, the existence of the nonzero (0 m/s) SPW lower bounds also indicate that nearly every high SPW “had” to be associated with a high Z.

These discrepancies indicate that while it is likely that the extreme small scale organization of these precipitation structures may generate considerable SPW (and an upper tail), it seems more likely that hardware effects play a dominant role in generation of these features in this particular data set. This possibility for system error was strengthened when analysis of clutter data at successively greater ranges resulted in similar Z-SPW distributions in which the first occurrence (lowest Z bin) of a lower bound shift in SPW moved to higher Z with increasing range. Thus, the identification of an “unusually” strong correlation of

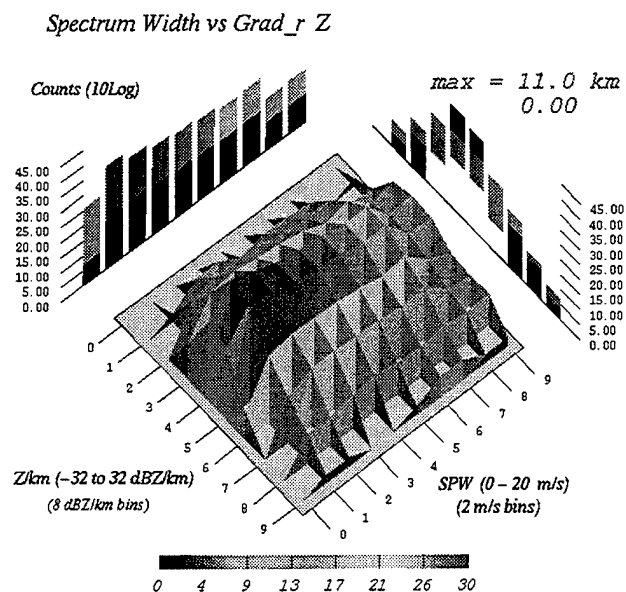


Figure 17a

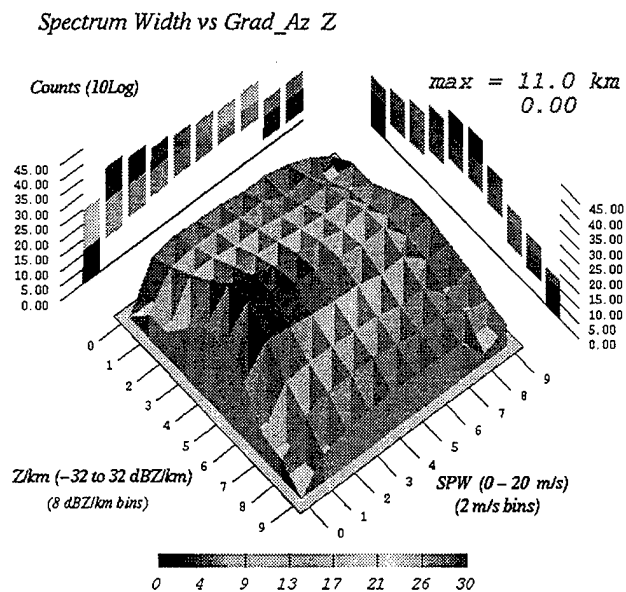


Figure 17b

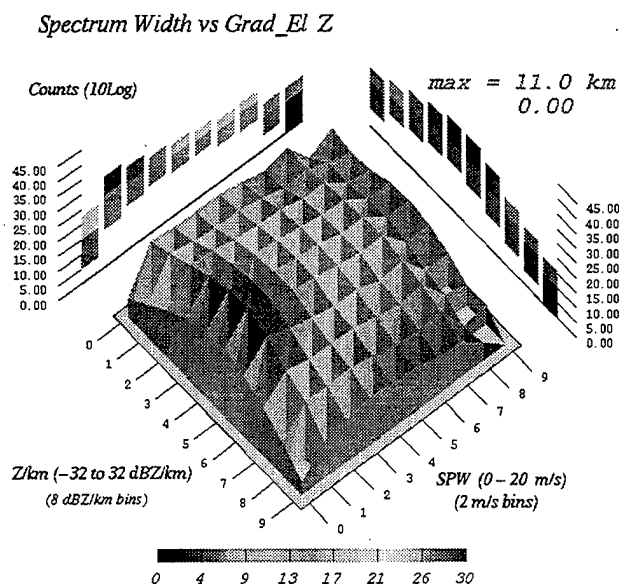


Figure 17c

Figures 17a-c. Example correlation distributions between collocated SPW and 1D gradients of Z for a single storm for Melbourne, FL WSR-88D on 03/26/92 (MLB221). Despite very large 1D gradients in Z (Figures 1a-c), SPW appears generally uncorrelated with Grad Z. Format same as Fig. 10.

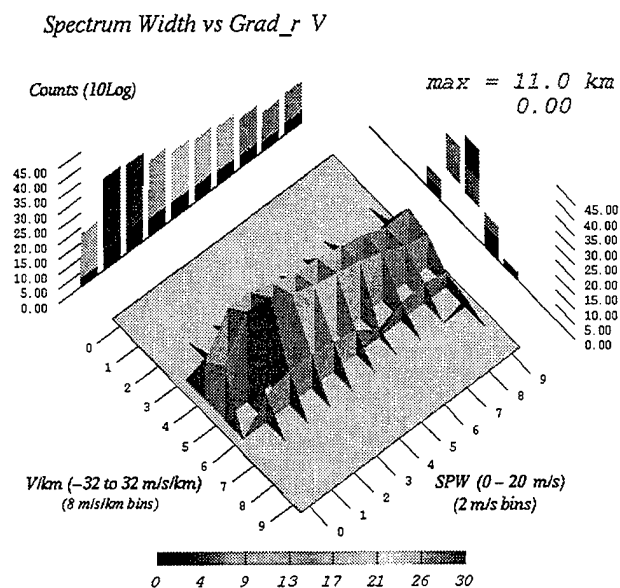


Figure 17d

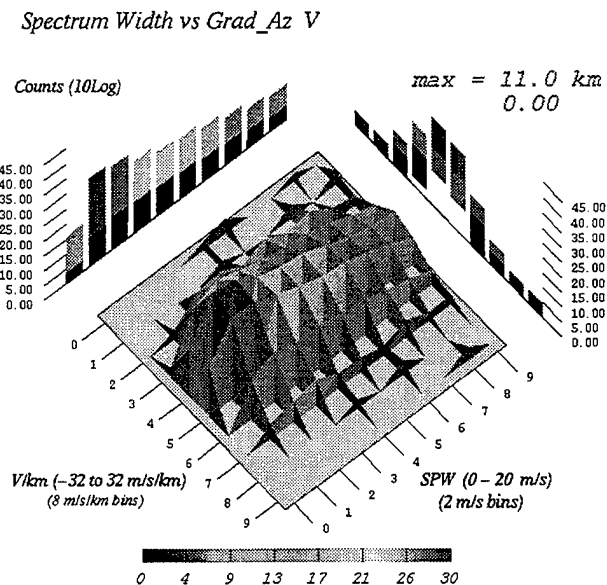


Figure 17e

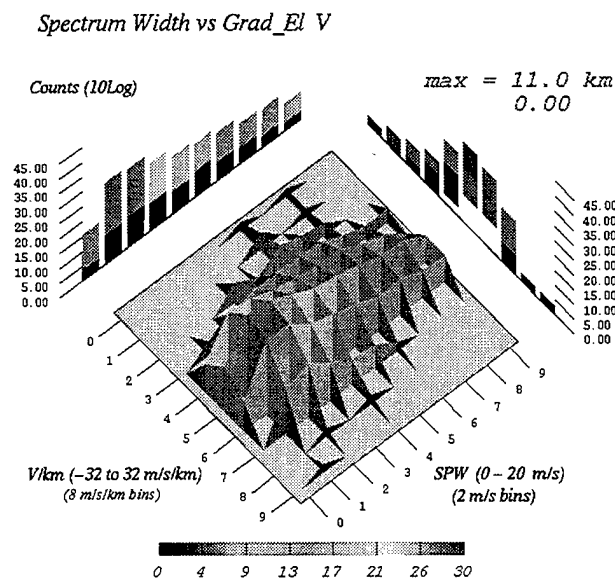


Figure 17f

Figures 17d-f. Examples of correlation distributions between collocated SPW and 1D gradients (radial, azimuthal, elevational) of V for a single storm for Melbourne, FL WSR-88D on 03/26/92 (MLB221). Despite very large 1D gradients in V (Figures 17d-f), strong correlations with SPW are not observed. Format same as Fig. 10.

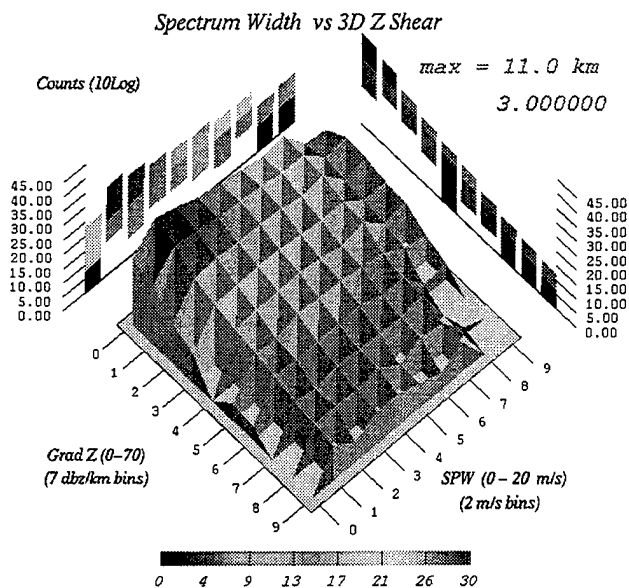


Figure 17g

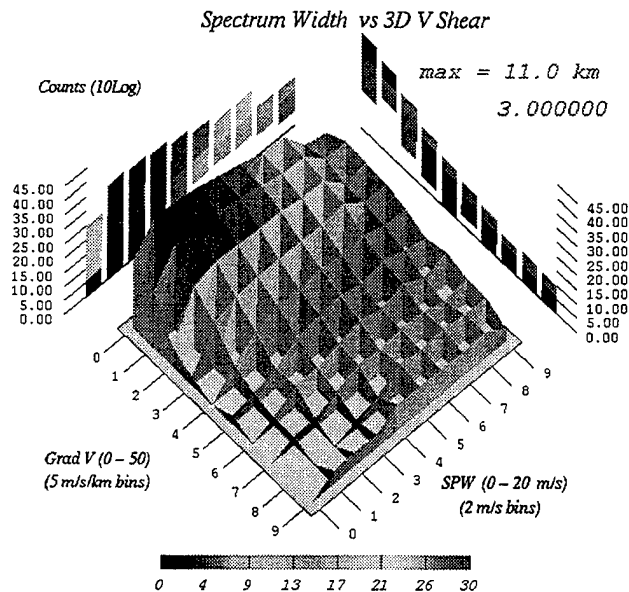


Figure 17h

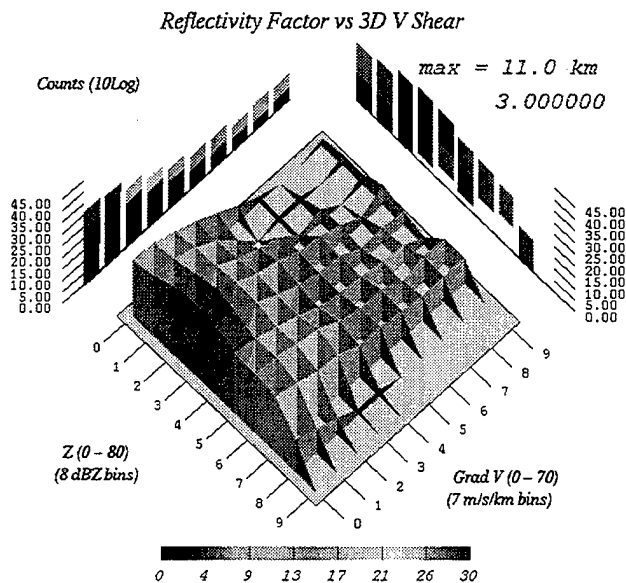


Figure 17i

Figures 17h-i. Example correlation distributions between collocated SPW and 3D gradients of Z and V for a single storm for Melbourne, FL WSR-88D on 03/26/92 (MLB221). Correlation with 3D gradient of Z (Figure 17g) is not seen, but is seen between SPW and 3D Grad V (Figure 17h). Note SPW minimum bound shifting away from $SPW = 0$ m/s roughly as $SPW = (.3KRT)SQRT(3)$. Also, the strong correlation between Z and 3D Grad V (Figure 17i) shows large V shears exist primarily in regions of high Z. Format same as Fig. 10.

SPW with Z may be sufficient to indicate that the WSR-88D is experiencing a system problem that may affect the V, and especially SPW estimates.

In summary, these simple correlation analyses provide some useful insight into the degree of organization of the storm structures, the success of the WSR-88D in removing SPW artifacts from storm boundary, multi-trip, and clutter contaminated data, and an indication of gross system health. It strengthens the association between high SPW and storm boundary regions. Further analysis of SPW versus velocity shears should demonstrate the utility for assessing the relative importance of shear and turbulence within localized storm regions.

4 WSR-88D PROBLEM AREAS

The observations presented above clearly demonstrate that the WSR-88D SPW provides information that is useful in detecting and monitoring various storm features. However, concerns of hardware/software performance have also been noted, and thus the WSR-88D SPW parameter does not come freely without some negative baggage. This is expected, and is frankly why SPW is rarely utilized. Some areas noted for attention include:

- Ground clutter contamination
- Storm extensions via sidelobe
- Incorrect mapping of multi-trip data
- SNR thresholding near radar storm top and boundary
- Higher variability and mean values for second trip SPW data
- Enhanced SPW estimates ? (slow automatic gain control (agc) in V/SPW channel ?)
- Excessive broad range of SPW values

The observed clutter varies considerably between sites, with MLB generally exhibiting the greatest amount in both magnitude and areal coverage, with full 360 degree clutter out to a range of 10-20 km. The coastline is generally observable. The MLB221 data set is of particular concern, with hardware problems apparently responsible for enhanced clutter this day. Ground clutter contamination is not strongly observed in the DDC and LBB data but is

sufficient to influence algorithm performance out to 10 km. These data clearly indicate the need for greater clutter filtering capability, possibly with the use of a TDWR-like clutter residue editing map. The automated removal of enhanced SPW at the first/second trip range interface should be readily accomplished. However, data lying near this range interval may be corrupted beyond use.

Sidelobe contamination is a potential fact of life with radar data. False mappings of SPW data outside storm boundary are occasionally noted in the DDC and LBB data, but very little is observed in the MLB data. This is likely a result of a generally lower maximum Z in MLB data (< 64 dBZ) than observed at DDC and LBB (< 78 dBZ). These contamination areas are easily detectable, when present. The overall success of the WSR-88D to remove enhanced SPW generated in regions of low SNR at storm boundaries not associated with the core regions is generally high. It is clear that automated analysis methods must be able to recognize and account for these artifacts, and could likely be accomplished by correlating the local values of Z and SPW to ascertain whether a storm boundary condition exists. It is encouraging that 3-body hail signals can survive this data quality processing and leave a readily detectable signature that should allow for automated "large hail" detection.

Difficulties in correctly mapping data between the first and second unambiguous ranges for Doppler data is often noted, with the central cores of distant storms (beyond about 130 km) retained at their correct locations, but peripheral areas mapped into the first Doppler range interval. While much of the incorrectly mapped data are often recognized as clutter, when imbedded into first range interval storm data, it is difficult to detect and results in a greater variability in all three (Z/V/SPW) fields than in nearby regions. Elimination of such data from WSR-88D Archive Level II data may be quite difficult, pointing to the need for more accurate approaches to this problem during data acquisition processing.

The SPW data beyond the first Doppler velocity range interval occasionally displays a more highly speckled (random) appearance than first trip data. This may reflect the natural effect of inclusion of larger storm regions into single sample volumes, thereby allowing for incorporation of a greater range of Z/V gradient field components. Due to this increased randomness, 3D visualization and correlation analysis may be less successful at these greater ranges, suggesting that algorithms utilizing SPW (and V) may need to employ some form of

smoothing and range dependent logic.

It is curious that one of the apparent successes observed in these analyses was the detection of apparent 3-body scattering from large hail, particularly via the SPW data. The observation of an increasing (nonzero) minimum SPW with increasing Z in the Z-SPW correlation distributions suggests a hardware effect may be enhancing the SPW values. While clearly demonstrated for the MLB WSR-88D which admittedly was known to be experiencing clutter filter problems, there is an occasional hint of similar behavior with data from the other WSR-88D systems used in this analysis. The effect becoming more pronounced with increasing Z does seem to suggest a receiver problem. This may be one reason for hail spikes to appear greater in length in V/SPW data than in Z data. A cursory analysis of WSR-88D Z/V/SPW hail spike data, however, suggests that a more reasonable explanation is that the WSR-88D color display scheme typically shows all V/SPW data, but a considerable portion of the spike (e.g. less than 0 dBZ) is not displayed. This implies that a lower displayable Z may be useful for enabling forecasters to visually detect the hail spike during normal operational periods. Whether accentuated or not, the 3-body spike is more easily detectable in the SPW data than in V and Z data, suggesting that SPW may be a very useful parameter in detecting large hail.

Data quality is an issue that always looms in the background when employing SPW estimates. As discussed earlier, there are many well known contributors (e.g. turbulence, Z/V gradients, antenna rotation, fallspeeds, clutter filtering, etc.) to SPW, and more subtle and unknown adversaries (e.g. hardware misalignments, poor implementation of pulse pair processing) that may add "noise" to the data streams. The variability in the range of SPW values is generally acceptable, often within 0 - 8 m/s, occasionally very large (0 - > 12 m/s) and sometimes astonishingly large (0 - >16 m/s). That such high values and variability are observed is disconcerting, but not necessarily an impediment to the "automated" use of SPW. As noted, generally the "patterns" or "organized regions" of high SPW provide the clues to important storm processes and feature detections, and these are most often found precisely when the storms themselves become highly organized. Pattern detection may employ (floating) thresholds appropriate for the storm, or region, being analyzed. Floating thresholds may be derived from the population of SPW estimates within that specific storm region. The high variability in SPW values between storms, and during storm development, make the

combined use of values and patterns necessary.

5 SUMMARY

Within this limited study the SPW is seen to provide useful information in identifying a number of storm hazards such as wind shift lines and very large hail. In addition, the development of 3D SPW structures would appear to provide clues for locating regions of enhanced shear and turbulence without actually performing the gradient field calculations. The SPW structures appear to vary with the evolution of the storm precipitation structures, suggesting further analysis should continue the search for SPW precursor signatures.

More specifically, the detection of shallow wind shift features (e.g. gust front and thin lines) is particularly useful for forecasting new storm initiation. Their detection via SPW is occasionally observed to be superior than through use of Z, V, or V shears alone. The SPW signature develops in response to both the turbulence and wind shear present within the radar pulse volume. Because of the three-dimensional nature of turbulence, there will generally be a turbulent contribution to the SPW. However, wind shear is more two-dimensional, and both its measurement and contribution to SPW are a function of the angles between the wind vectors and the radar viewing direction. Thus, there may often be an SPW signature even while the signatures in Z, V, or V shear fields are weak.

Detection of the apparent 3-body scatter (large hail) spike is a clear success, with the SPW signatures more discriminating than Z signatures. Use of this feature is an important asset since hail detection efforts have traditionally been directed towards detecting a Z signature, or identification of when Z exceeds a high threshold value. This has been a natural consequence of the necessity to monitor reflectivity factor (Z) displays to observe storm evolution, and the little attention and great skepticism traditionally given to SPW data. However, these observations suggest that the SPW spike may be the more easily detected hail signature, and when in the presence of a collocated Z spike is likely a clear indication of the presence of very large hail.

There is clearly an indication of increased SPW structure when the storm Z and V

structures are more organized. This is particularly well observed in Melbourne, FL data where striking precipitation structures are accompanied by strong and organized SPW, structures. Unfortunately, suspected system problems make full investigation of the fascinating aspects of these data difficult.

There are obvious system areas that need improvement, including more accurate multi-trip resolution, clutter filtering and/or residual clutter removal, and perhaps greater receiver gain control. The current impact on SPW data is the loss of SPW integrity (isosurfaces, field means and maximums and structure) within storm regions, loss of useful data near the radar, and introduction of false echoes. Without modifications, many of these SPW data artifacts may still be recognizable by automated means. Such methods would require the monitoring of storm boundaries, the removal of the ring of contaminated data at the first Doppler unambiguous range, and the generation of a updated ground clutter map. It is possible that simple monitoring of the Z - SPW correlation distribution may provide a means for automatically monitoring data quality and selecting appropriate SPW decontamination procedures.

The current results were derived through observation of the structures clearly visible in 3D visualization, and the correlation of SPW against collocated radar parameters such as Z, V, and their gradient components. The next phase requires the monitoring of these features over time to tie them to storm evolution and forecasting. This will require correlation with additional storm parameters such as storm mass and height, maximum Z and its location, shear zones, vertical drafts, and hazards such as hail, wind shift lines, mesocyclones and weak echo regions, all on a large database. The development of automated methods for detecting the currently observed features such as 3-body scatter for detection of very large hail, and surface wind shifts should also be undertaken.

6 BIBLIOGRAPHY

A.R. Bohne, "The Joint Agency Turbulence Experiment - Final Report", AFGL-TR-85-001, ADA160420

A.R. Bohne, "Radar Detection of Turbulence in Precipitation Environments", Journal of the Atmospheric Sciences, **39**, 1982, pp1819-1837

Dixon, M., and G. Wiener, "TITAN: Thunderstorm Identification, Tracking, Analysis, And Nowcasting - A Radar-Based Methodology", Journal of Atmospheric and Oceanic Technology, **10**, 1993, pp785-797

Hermes, L.G., Witt, A., Smith, S.D., Klinge-Wilson, D., Meinis, D., Stumpf, G.F., and M.D. Eilts, "The Gust Front Detection And Wind-Shift Algorithms For The Terminal Doppler Weather Radar Systems", Journal of Atmospheric and Oceanic technology, **10**, 1993, pp693-709

M. Pedder, "Interpolation And Filtering Of Spatial Observations Using Successive Corrections And Gaussian Filters", Monthly Weather Review, **121**, 1993, pp2889-2902

Roberti, L., and G. Perona, "Ground Clutter Removal And Data Coding In Radar Meteorological Maps", IEEE Transactions on Geoscience and Remote Sensing, **31**, 1993, pp1260-1264

Tung, S.-L., Smalley, D.J., Harris, F.I., Desrochers, P.R., and A.R. Bohne, "Evolution of Three-Dimensional Frontal Structure" , Preprints, 27'th Conference on Radar Meteorology, American Meteorological Society, Boston, MA, 1995

Wilson, J. W., and C.K. Mueller, "Nowcasts Of Thunderstorm Initiation And Evolution", Weather Forecasting, **8**, 1993, pp113-131

Wilson, J. W., and D. Reum, "The Hail Spike: Reflectivity And Velocity Signature", Preprints, 23'th Conference on Radar Meteorology, American Meteorological Society, Boston, MA, 1986

Xu, M., and T. Gal-Chen, "A Study Of The Convective Boundary Layer Dynamics Using Single Doppler Radar Measurements", Journal of the Atmospheric Sciences, **50**, 1993, pp3641-3662

D. Zrnica, "Three-body Scattering Produces Precipitation Signature Of Special Diagnostic Value", Radio Science, **1**, 1987, pp 76-86